



ELSEVIER

Coastal Engineering 41 (2000) 201–235

**COASTAL
ENGINEERING**

www.elsevier.com/locate/coastaleng

Spectral wave modelling with non-linear dissipation: validation and applications in a coastal tidal environment

Christoph Schneggenburger, Heinz Günther*, Wolfgang Rosenthal

Institute of Hydrophysics, GKSS Research Centre, Max-Planck-Str., D-21502 Geesthacht, Germany

Abstract

A spectral wave model with non-linear dissipation is validated and applied in wind-wave investigations in the Sylt–Rømø Bight. The model was developed for applications in small-scale shallow-water environments. Numerical experiments on wind waves in the bight demonstrate the applicability of the model in small-scale systems with time-varying water levels and currents. A 1-month hindcast of wind in the Sylt–Rømø Bight is used to successfully validate the model against field data. The influence of currents on wave parameters is reproduced quantitatively. It is shown that inclusion of currents distinctly improves the hindcast skill for wave periods. Case studies for prescribed wind situations reveal a significant complex interaction of tide- and wind-driven currents on wind waves. © 2000 Elsevier Science B.V. All rights reserved.

Keywords: Currents; Shallow water; Wave modelling; Wave spectra

1. Introduction

Research has, in recent years, become focussed on spectral wave models for coastal environments because an understanding of waves is desirable before we can answer the many questions related to coastal protection, environmental control and management, and sustainable development. The prediction of sea state is essential for the design of coastal protection constructions, ports, harbours, and navigational channels. Furthermore, it is commonly accepted today that the sea state is key to understanding coastal dynamical systems, which consist of coupled atmospheric, hydrodynamic, morphological, and biological subsystems. The sea state links these subsystems: it influences mass,

* Corresponding author. Fax: +49-4152-87-1565.

E-mail address: guenther@gkss.de (H. Günther).

momentum, and energy fluxes between atmosphere and water body (Donelan, 1995; Makin, 1998). It has a large impact on mobilisation of sediments (Ross, 1995; Soulsby, 1997). Besides directly influencing the suspended matter regime, this mechanism can, through waves, impact on water quality, as some classes of nutrients and pesticides may be attached to sediments and suspended matter. Additionally, modulation of the light regime in the water column may impact on the biology. Recent interest in coupled atmospheric, hydrodynamic, and sedimentary phenomena in the Sylt–Rømø Bight (EU MAST III project PROMISE) thus created the need for a coastal wave model suitable for application to complex tidal systems with coupling between the atmospheric, hydrodynamic, and suspended-matter subsystems.

In the last decade, spectral wave models for the open oceans and shelf seas have reached a high standard (Cardone and Resio, 1998). Examples of such models are WAM (WAMDI, 1988), its current version WAM-cycle4 (Günther et al., 1992), and WAVEWATCH (Tolman, 1991; Tolman and Chalikov, 1996). Research on spectral models for coastal applications is currently in progress. One particular example is the stationary near-shore model SWAN (Holthuijsen et al., 1993; Ris, 1997; Booij et al., 1999; Ris et al., 1999). It is applicable to situations where incident waves travel through the region of interest in a time interval much smaller than the intrinsic time scales of the system, e.g. tidal variation of water levels and currents. Besides wave generation, dissipation, and non-linear transfers, SWAN optionally allows further processes, which can be important in shallow water, to be considered, e.g. depth-induced wave breaking and triad interactions of waves. A ‘non-stationary’ version of the model is being developed. A high-resolution small-scale version of WAM has been introduced by Luo and Sclavo (1997) and Monbaliu et al. (2000) (this volume). In this version of WAM, numerical adjustments related to the small scales have been carried out.

A wave model with a non-linear dissipation source function accounting for dissipation by wave-turbulence interaction (Rosenthal, 1989) has been introduced by Schneggenburger et al. (1997), based on a 1D version by Günther and Rosenthal (1995). The model is called the K-model and was developed for applications in coastal systems. In this model, only essential physical processes are considered in order to limit the model complexity, whereas SWAN and WAM considers, in detail, non-uniform and non-stationary media, which are common in coastal tidal environments. Processes considered are wind input by Snyder and Phillips mechanisms, non-linear dissipation, and bottom-interaction dissipation. Depth-induced wave breaking is not significant in the applications described in this paper, although it can be essential in other systems. A corresponding source term has yet to be included in the K-model. Quadruplet interactions of waves in small-scale non-uniform systems may be neglected (Schneggenburger, 1998). We do not claim that non-linear energy transfer in the development of ocean wave spectra is less pronounced in wind wave development in coastal systems (see, e.g. Hasselmann, 1962; Phillips, 1981; Young and van Vledder, 1993; Lin and Perrie, 1997; Cardone and Resio, 1998; Young, 1998). The reason for disregarding quadruplet interactions is that this theory was developed for strictly homogeneous systems, a prerequisite that is definitely violated in coastal areas. Hence, use of a numerical parameterisation according to this theory can, in certain cases, lead to substantial errors in applications to inhomogeneous systems. In the absence of a suitable theory and

related parameterisation, this insight justifies the neglect of non-linear energy transfer processes in coastal wave modelling. A consequence of omitting quadruplet interactions is a considerable reduction in computing cost.

The advantage of the K-model over SWAN (i.e., the complexity of source terms is limited) enhances its general applicability and use as a forecast model: calibration by including or excluding various processes to achieve optimum performance in a specific application is not necessary. The K-model was originally calibrated to selected empirical small-scale wave growth laws (Hasselmann et al., 1976). An advantage of the K-model with respect to WAM (in applications to coastal environments) is the use of an explicit dissipation source function. In WAM, the dissipation source function is parameterised following Komen et al. (1994) to close the energy balance of the other source terms.

The aim of this paper is to validate the K-model in a coastal environment with tidal influence, use this validated model to investigate the influence of currents on wind waves and thus decide whether or not to include currents in wind-wave analyses of such systems. The plan is to carry out a long (1 month) hindcast of wind waves in the Sylt–Rømø Bight to enable a statistically robust validation to be made against wave data. The influence of currents is made apparent by comparing wave model runs with and without current input. Case studies for prescribed wind situations are used to qualitatively investigate the influence of currents. Statistical validation for both wave model hindcast runs (with and without currents) are used for a quantitative analysis of current impacts.

An important result from this study is the successful validation of the K-model-quantified by means of hindcast skill. Furthermore, depending on time, location and weather situation, the impact of currents on wind waves was considerable. Based on this result, we concluded that the inclusion of currents is recommended. The hindcast skill for period parameters was distinctly improved by including currents.

The structure of the paper is as follows. Section 2 covers tools and methods of investigation, including a description of the K-model. Characteristics of the Sylt–Rømø Bight important in the investigation are listed. The procedure used in the investigation is outlined. In Section 3, results of the hindcast, statistical validation, and the case studies are presented. The discussion in Section 4 covers selected aspects of the model results. The conclusions of the study are given in Section 5. Notes on the current modelling effort in the Sylt–Rømø Bight are included in Appendix A. These results were used as input fields for the wave model in the applications presented here.

In the mathematical formulae presented, vectors appear in bold type. Their scalar product is denoted by a central dot. Partial derivatives with respect to time t appear as ‘ ∂_t ’. Gradients with respect to, say location x , are denoted by ‘ ∂_x ’.

2. Tools and methods of investigation

2.1. Description of the K-model

The K-model is a discrete spectral wave model. It solves the wave action balance equation in k -space, with the wave vector modulus and direction (k , θ) in polar

coordinates as independent variables. In flux form, the balance equation for the wave action density $N \equiv E/\sigma$ in polar coordinates is

$$\partial_t + \partial_x \cdot (\dot{x}N) + \partial_k \cdot (\dot{\mathbf{k}}N) + \partial_\theta \cdot (\dot{\theta}N) = S(N). \quad (1)$$

Here, E and σ are the wave energy density and wave intrinsic frequency. N , E , and σ are functions of the wave vector coordinates (k, θ) , and of location x and time t . The arguments have been dropped in our notation for clarity. $S(N)$ is the sum of sources of action density. In the K-model, the sum is

$$S(N) = S_{\text{in}} + S_{\text{phil}} + S_{\text{dis}} + S_{\text{bot}}, \quad (2)$$

consisting of a modified Snyder wind input S_{in} , Phillips wind input S_{phil} , non-linear dissipation S_{dis} , and bottom-interaction dissipation S_{bot} . For further concepts and terminology of wave theory and modelling see Komen et al. (1994).

2.1.1. Source functions

Modified Snyder wind input, Phillips input and non-linear dissipation are listed in detail below. For further discussion and details on all source functions, see Schneggenburger et al. (1997) and Schneggenburger (1998).

The Snyder wind input (WAMDI, 1988) was modified to include the effect of wind ‘gustiness’.

$$S_{\text{in}} = \beta\sigma GN(\mathbf{k}). \quad (3)$$

The gustiness parameter G was chosen as in Komen et al. (1994):

$$G = \frac{\sigma_{u_*}}{\sqrt{2\pi}c_*} \exp\left[-\frac{c_* - u_*^2}{2\sigma_{u_*}^2}\right] + \frac{1}{2} \left[\frac{u_*}{c_*} - 1\right] \left[1 - \Phi\left(\frac{c_* - u_*}{\sigma_{u_*}}\right)\right] \quad (4)$$

with

$$c_* \equiv \frac{\sigma}{28k\cos(\theta - \theta_w)} \quad (5)$$

in the case of $\cos(\theta - \theta_w) > 0$, otherwise $G = 0$. In Eq. (4) the probability function

$$\Phi(x) \equiv \frac{2}{\sqrt{2\pi}} \int_0^x e^{-\frac{1}{2}t^2} \quad (6)$$

appears. The quantity σ_{u_*} is the standard deviation of the assumed normal distribution for the friction velocity. The parameters of the Snyder input are

$$\beta = 0.0009, \quad \frac{\sigma_{u_*}}{u_*} = 0.4. \quad (7)$$

In the K-model’s present state of development the friction velocity in the input source functions was replaced by the wind speed at 10 m height, using the fixed relation

$28u_* \rightarrow 1.2u_{10}$. This was obtained by tuning the peak frequency of the deep-water fully developed spectrum.

The non-linear dissipation function in the K-model is given by

$$S_{\text{dis}} = -\gamma g k^5 \left(\coth 2kh + \frac{kh}{\sinh^2 kh} \right) N^2(\mathbf{k}). \quad (8)$$

The symbols g , k , and h denote the gravitational acceleration, modulus of the wave vector, and local water depth, respectively. The dissipation parameter is a function of N and the spectral mean wave number $\langle k \rangle$, and thus generates a coupling between different ‘bins’ in the model:

$$\gamma(N) = \gamma_0 \frac{p_1 \left(p_2 \frac{k}{\langle k \rangle} \right)^q + 1}{\left(p_2 \frac{k}{\langle k \rangle} \right)^q + 1} \quad (9)$$

with the parameters

$$\gamma_0 = 0.09485, \quad p_1 = 10.0, \quad p_2 = 1.6, \quad q = 6.0. \quad (10)$$

This function parameterises the enhanced dissipation of short waves in a wave spectrum: it is an increasing function of $k/\langle k \rangle$, with minimum γ_0 and maximum $p_1\gamma_0$. The parameter p_2 adjusts the location of the ascent in k relative to the mean wave number $\langle k \rangle$. Both p_2 and q control the steepness of γ in k . Further details can be found in Schneggenburger (1998).

The Phillips input source function S_{phil} is based on the version of Cavaleri and Rizzoli (1981), and modified by Tolman (1992). To reduce the input for short waves in small-scale applications, the source function was re-scaled to one-tenth of its original magnitude and a further filter was applied (Schneggenburger, 1998):

$$S_{\text{phil}} = 0.1 \times 2 \frac{80\rho_a^2}{g^2\rho_w^2} \frac{c_g}{\sigma} [u_* \cos(\theta - \theta_w)]^4 \exp \left[- \left(\frac{f}{f_{\text{PM}}} \right)^{-4} \right] \exp \left[- \left(\frac{f}{f_{\text{PM}}} \right) \right]. \quad (11)$$

Tolman filter new filter

Here, ρ_a and ρ_w are the densities of air and water, f and f_{PM} are frequency and Pierson–Moskowitz frequency (Pierson and Moskowitz, 1964), and c_g is the intrinsic wave group velocity.

The bottom-interaction dissipation function was taken from Hasselmann et al. (1973). The interaction parameter in this formulation is $\Gamma = 0.038 \text{ m}^2 \text{ s}^{-3}$.

The numerical implementation of source functions in the K-model was adopted from WAM cycle-4. It is a time-centred implicit scheme with approximations to facilitate computations (WAMDI, 1988). Unlike WAM cycle-4, one can choose a source-term

integration time step that is longer than the propagation and refraction time steps. The same feature has been reported as a modification of WAM cycle-4 by Monbaliu et al. (2000, this volume). The K-model was calibrated to match growth curves as in Hasselmann et al. (1976), up to the (normalised) fetch of $gx/u_{10}^2 = 10^4$.

All source functions in the K-model depend on local water depths, either explicitly or implicitly via circular frequencies, phase and group velocities. However, possible effects of currents on the source functions has, until now, been disregarded in the K-model, since quantitative knowledge about this has not been established. In particular, the input source functions S_{in} and S_{phil} do not take into account the relative speed of winds and currents. This can be seen in Eqs. (5) and (11), which contain the intrinsic frequency σ instead of absolute frequency ω . The choice was made to avoid peculiar effects such as wind-wave generation in case of zero winds and strong currents.

2.1.2. Propagation and refraction

Propagation and refraction in a discrete spectral wave model are represented by the \mathbf{x} and \mathbf{k} gradient terms in Eq. (1). Since a flux-type balance equation is shape-invariant when a coordinate transformation is applied to \mathbf{x} and \mathbf{k} , the explicit propagation and refraction terms in the model are specified completely by the ‘dot terms’ corresponding to the chosen set of physical and wave vector-space coordinates. The dot terms are obtained from the dispersion function Ω for linear water waves and the Hamilton equations (see e.g. Komen et al., 1994). In this model, the dot terms \dot{x}_1 , \dot{x}_2 , \dot{k} , and $\dot{\theta}$ need to be determined. The location dot terms are directly identified as components of the wave group velocities. The group velocities consist of two terms: the intrinsic wave group velocities $\partial\sigma/\partial k$ and the superimposed current velocities, which thus appear in the dynamical equation for the wave action density.

For the wave vector dot terms a short calculation leads to explicit formulae, which indicate a further influence of external fields on the wave dynamics:

$$\begin{aligned}\dot{k} &= -(\sin\theta\partial_{x_1}\Omega + \cos\theta\partial_{x_2}\Omega), \\ \dot{\theta} &= -(\cos\theta\partial_{x_1}\Omega + \sin\theta\partial_{x_2}\Omega)k^{-1}.\end{aligned}\quad (12)$$

The dispersion function Ω depends explicitly on water level fields $h(\mathbf{x}, t)$ and current fields $\mathbf{u}_c(\mathbf{x}, t)$:

$$\Omega(\mathbf{k}, \mathbf{x}, t) = (gk \tanh kh(\mathbf{x}, t))^{\frac{1}{2}} + \mathbf{k} \cdot \mathbf{u}_c(\mathbf{x}, t). \quad (13)$$

Therefore, derivatives of water levels and currents are included in the action balance equation. Note, however, that only spatial derivatives of the dispersion function appear in Eq. (12). If frequency and direction are used as independent variables, partial time derivatives of the dispersion function will also appear. The K-model formulation is well adapted to tidal systems because the non-stationary dynamical equation can be solved without the need to compute time derivatives of water level and current fields. A disadvantage of the (k, θ) formulation can be seen in the $\partial_k(\dot{k}N)$ term in Eq. (1).

Spectral energy fluxes in k -direction caused by shoaling lead to an effective loss of resolution, because transfer of energy from small to larger k -values will gradually confine the energy-containing part of the spectral grid. Also, these energy fluxes will impose stability requirements in the numerical treatment, cf. the choice of time steps in Section 2.3.

Propagation and refraction are implemented in the K-model with first-order upwind schemes. Since water levels and currents appear in the dispersion function in different terms, propagation, depth refraction, and current refraction can be treated in separate subroutines with individual time steps. The Courant–Friedrichs–Lewy (CFL) stability criterion is checked in its exact form. The individual terms of the CFL number can be identified separately. This enables an educated choice of time steps for the propagation routine and refraction routine.

2.1.3. Influence and treatment of non-stationary water level and current fields

Non-stationary external fields are taken into account in the K-model by replacing the stationary fields in the action balance Eq. (1) by time functions. These can cause modulation of wave parameters by the following mechanisms.

1. Space-local effects, i.e. depending only on local values of the external fields:
 - (a) Variation of current-induced Doppler shifts of integrated period parameters and energy-conserving shifts within the wave spectrum.
 - (b) Influences of water-depth variation on local wind input and dissipation.
2. Non space-local effects:
 - (a) Variation of shoaling and refraction.
 - (b) Variation of fetch due to up-fetch dry-falling areas.
 - (c) Variation of effective fetch through current-advected wave energy propagation.

Some of the effects resulting from space- and time-varying external fields can be scaled and quantified individually, but the net result of their complex interaction is hard to assess. These net effects can be investigated by case studies with a wave model.

Some technical details on the treatment of non-stationary water levels and currents in the K-model are given below. Wet points in the model topography can be temporarily dry due to time-changing water levels. In the K-model, water levels below 0.5 m are treated as dry points. The choice of a minimum water level of 0.5 m was supported by considering the water level variability within a grid box of the given horizontal dimensions. With decreasing depth it becomes more likely that a part of the grid box is dry in reality. Such grid points should be excluded from the calculations. At dry points in the wave model grid, the wave energy is set to zero after every propagation time step.

The CFL stability criterion for the first-order upwind propagation in (x, k) -space must be observed whenever new water level fields and current fields are provided.

For a convenient comparison with measurements and other models, fields of energy density E in (f, θ) coordinates are desirable model outputs. In the K-model, the action density spectra are transformed to energy densities at each output time and location. The energy spectrum has fixed frequency and direction axes at all locations and times. The

transformation is performed using an energy-conserving method. However, energy situated beyond the chosen output frequencies is lost.

Wave modelling using the dynamical Eq. (1) in (k, θ) coordinates is well suited to situations in which strong opposing currents are present, when wave blocking can occur. There are no formal restrictions on the current velocity in our formulation, e.g. singularities in Jacobians or related problems. Since the wave numbers of plain waves are not changed by currents, the wave blocking feature is only employed in post-processing, when energy spectra in frequency direction coordinates are calculated at specified output locations and times. The treatment is straightforward: if negative absolute frequencies occur, the corresponding directions are reversed. Energy located close to the frequency origin is removed to avoid division by small numbers or zero.

2.2. The Sylt–Rømø Bight

The Sylt–Rømø Bight is located in the North Sea coast adjacent to the Danish–German border. The bight is enclosed by the islands Sylt and Rømø. Both are connected to the mainland by artificial dams. The bathymetry of the bight is shown in Fig. 1. The bight is approximately 30 km long and 20 km wide. The opening to the North Sea

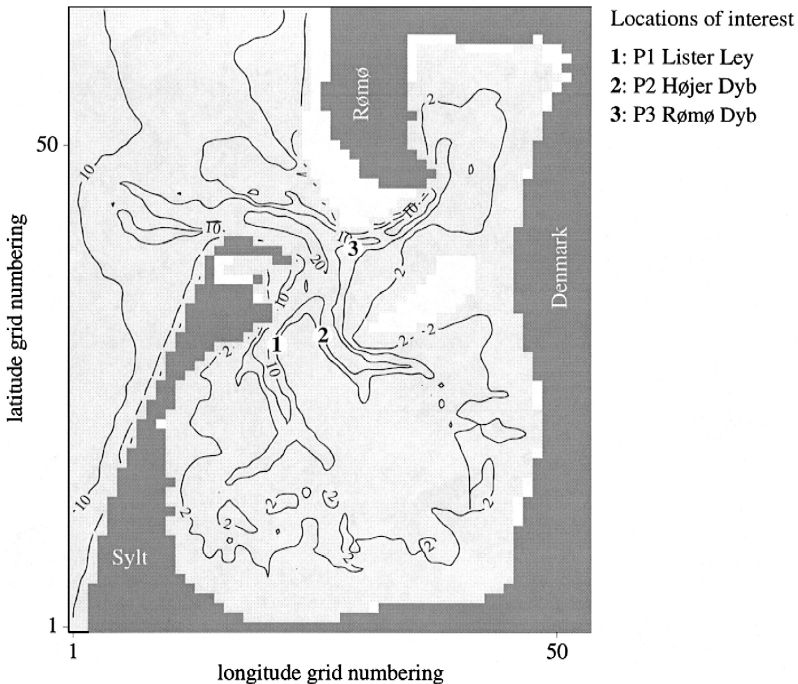


Fig. 1. Bathymetry of the Sylt–Rømø Bight. Land points are dark grey, dry sea points are white, and wet sea points are light grey. Water depths represent levels at a select high tide. Contours show depths of 2, 5, 10, and 20 m. Numbers in bold type indicate three field stations of interest.

between Sylt and Rømø has a width of about 3 km. This opening is the only tidal inlet into the bight. There are three tidal channels within the bight with water depths from 5 to 10 m. The remaining parts of the water body are less than 3 m deep. Up to 40% of the area dries out at low tide. The tidal range is approximately 2.3 m. Tidal currents can have velocities of up to 2 m s^{-1} in the inlet. In the tidal channels the current velocities are usually less than 1 m s^{-1} . The currents over the tidal flats are weak compared to those in the channels. Fig. 1 indicates the location of three measurement stations. The Sylt–Rømø Bight was chosen as test area of the K-model for a number of reasons.

(1) There is only one narrow opening to the North Sea, the wave regime in the Sylt–Rømø Bight is expected to be dominated by locally generated wind waves. Waves over flooded tidal flats will be depth-limited. The wave group velocities resulting from the short fetches will be of the same order of magnitude as the current velocities. For this reason, a considerable influence of the tidal currents on the waves is expected.

(2) The opening of the bight to the North Sea is particularly suitable for realistic current modelling. A current model can be driven with measured water levels at the bight entrance, as is described in Appendix A.

(3) Recent interest in suspended matter dynamics and morphology of the bight creates the demand for wave modelling in the area, enabling the prediction of mobilisation of sediments by wave bottom interactions.

(4) Wave model results can be validated using measurements from recent field campaigns carried out within PROMISE by GKSS-Forschungszentrum, Geesthacht.

2.2.1. Time-scale analysis to show that the wave field is non-stationary

The sea state in the Sylt–Rømø Bight is essentially non-stationary and thus requires non-stationary wave modelling. The significance of time variations of external fields for the sea state in a given area of investigation must be checked with a scale analysis. A characteristic time scale of the wave field is the travel time of typical waves, say waves at the peak of a typical spectrum, through the relevant system. The travel time can be estimated as the ratio of the spatial dimension of the system to the peak group velocity, which describes the dominant propagation velocity of spectral wave action. Typical time scales for variation of external fields can be deduced from measurements. Stationary treatment will be possible if

$$\frac{\text{travel time}}{\text{time scale of variation}} \ll 1. \quad (14)$$

To carry out the analysis, we estimate the orders of magnitude of the scales for the Sylt–Rømø Bight. The wave regime in the bight is dominated by locally generated wind waves with peak frequencies as low as 0.2 Hz. This can be inferred, for example, from measurements given in Section 3. Corresponding group velocities at the peak frequency are below 5 m s^{-1} . The width of the bight is roughly 20 km, so the time taken for a spectral wave to travel through the bight is longer than 1 h. Measurements of currents, in Fig. 3, show that substantial changes can occur within 1 h. The ratio of travel time to time scale of the variation of the medium is thus of order one. It follows that it is inappropriate to treat wave modelling in the Sylt–Rømø Bight as stationary.

2.3. Investigation procedure

2.3.1. Numerical experiments

Numerical experiments have been performed to test and validate the model in a small-scale coastal application, and to investigate the current influence on wind waves in such systems.

(1) A 1-month wave hindcast in the Sylt–Rømø Bight was performed to allow a statistical validation of the model against field measurements of wave parameters within the bight. Furthermore, current effects were quantified in a realistic hindcast by comparing outputs of the model with and without currents. The relevance of current impact on the waves in this system was assessed in an objective manner by comparing the corresponding validation statistics.

(2) In case studies for the two different prescribed wind situations — 20 m s^{-1} east and northwest — the impact of tide- and wind-driven currents on wind waves in the Sylt–Rømø Bight was investigated. Again, wave model runs were performed with and without current input. This enabled the direct identification of current effects by comparing time series, parameter fields, and two-dimensional wave spectra from the two model runs. The time spans of the case studies were fixed by the available current and water-level fields from the current atlas of Behrens et al. (1997). Two days in February 1994 for the east 20 m s^{-1} (E20) case, and 3 days in June 1994 for the northwest 20 m s^{-1} (NW20) case.

2.3.2. Set-up of model system

Wave modelling in the Sylt–Rømø Bight must be performed as part of a model system. Current modelling is necessary for specifying water levels and the distribution of tidal flats, even if the influence of currents on waves is of minor importance. To this end, the current model TRIM (Casulli and Cheng, 1992; Casulli and Cattani, 1994) was applied. Details can be found in Appendix A. A description of the K-model set-up for the numerical experiments is given below.

(1) A $500 \text{ m} \times 500 \text{ m}$ resolution grid was chosen, see Fig. 1. A finer model grid may be desirable for studying the spatial variability of the water level and current fields within the Sylt–Rømø Bight. However, the need of computing resources for the long hindcast period of 1 month imposed a limit to resolution.

The chosen bathymetry is a coarser version of the current-model bathymetry. It was obtained by extracting data from every fifth grid point of the $100 \times 100 \text{ m}$ grid. Grid points representing the field stations were taken as the fine-grid points closest to the actual location of the stations to ensure correct local properties of the current and water level fields.

Data from single fine-grid points were favoured over averaging of fine-grid points within a coarse-grid box to avoid smoothing of the current field. Such smoothing can lead to an undesirable reduction in local current impacts on the wave field.

(2) The K-model spectral resolution was 12 directions and 25 wave numbers. The output frequency axis ranged from 0.1 to 1 Hz for the hindcast, and from 0.04 to 1 Hz for the case studies. The spectral directions were shifted to avoid propagation directions into principal grid directions. A better directional resolution, using 24 instead of 12

directions, is advisable but was not adopted in this study in favour of a long hindcast period and to save computing resources.

(3) The source term integration time step was 60 s. Propagation, current-refraction, and depth-refraction time steps were 20, 20, and 4 s, respectively. The small depth-refraction time step is caused by large depth gradients. This is not a major obstacle, since depth refraction is only a small part of all propagation and refraction computations. The ratio of the source time-step to propagation time-step was kept sufficiently small to avoid oscillatory peaks in the model results. These can be observed if large deviations from the self-similar shape of the spectra occur in between source term integrations.

(4) The stationary and homogeneous wind input is $u_{10} = 20 \text{ m s}^{-1}$ with directions (coming from) east and northwest. In the hindcast experiment, the wind measured at station P3 Rømø Dyb (see Fig. 1) was transformed to u_{10} assuming a logarithmic profile and the Charnock relation to provide the roughness length (e.g. Komen et al., 1994). These modified wind data were applied homogeneously with a time step of 15 min. No time interpolation was performed.

(5) Water levels and currents were provided from the TRIM runs. The 100-m output resolution was reduced to the wave-model resolution by selecting the same fine-grid points as for the bathymetry (see paragraph 1). Water depths at the grid boxes representing the field stations P1 Lister Ley and P3 Rømø Dyb were adapted to the measured values by adding a time-independent offset of a few tens of centimetres to ensure correct local processes for the wave modelling. The offset reflects the sub-scale variability in the 100-m resolution of the bathymetry.

The water-level and current input time-steps were 15 min, no time interpolation was performed. Beyond the boundary of the current-model grid at the bight entrance, zero currents and stationary water levels were prescribed.

(6) Boundary spectra for the hindcast study were provided from a North Sea 30×30 km resolution K-model run. Details of the model set-up and a validation exercise of the K-model on North Sea scales are described in Schneggenburger et al. (1997). The model was driven with German Weather Services (Deutscher Wetterdienst, DWD) Europe-model six-hourly wind fields. The spectra from a corresponding grid point of the North-Sea model were transformed to match the (k, θ) axes of the small-scale model, and distributed to all boundary points with water depths larger than 3 m. The boundary-value input time step was 15 min.

(7) For the east-wind case study, boundary spectra were obviously not needed. For the northwest-wind case, a matching date from the hindcast period was selected to obtain a realistic boundary spectrum.

3. Results

3.1. April 1997 hindcast

3.1.1. Meteorological situation

The surface-wind situation in the Sylt–Rømø Bight for April 1997 is illustrated in Fig. 2. The figure displays measured 10-min-average wind velocities and directions at

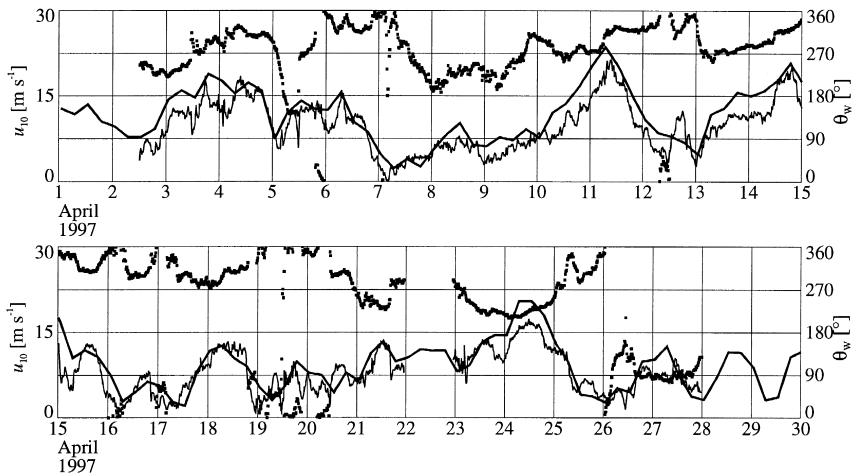


Fig. 2. Measured wind velocities at pile P3 Rømø Dyb (thin lines). For comparison, DWD six-hourly analysed wind velocities are shown as thick lines. Dotted data points are measured wind directions (right hand side y-axis, in meteorological convention — direction from which the wind comes).

pile P3 Rømø Dyb. Six-hourly analysed winds according to the DWD Europe model are given for comparison. The period April 1997 was chosen because the meteorology was dominated by strong winds and thus promised interesting sea-state situations. Measured wind speeds at 10 m height exceeded 15 m s^{-1} on 6 days. Major peaks occurred on the 11th, 14th, and 24th of April. The first two were above 20 m s^{-1} . Wind speeds above 10 m s^{-1} were from directions between west and north in most cases. The peak on 24th April was from a southwest direction.

Westerly wind directions in the period considered required the use of boundary spectra for the wave model to account for incoming waves from the North Sea. From a comparison of time variability of the measured and DWD model winds, it was obvious that higher resolution winds were needed for the wave modelling than the DWD Europe model can provide. Therefore, measured winds were processed for inputs as wind fields for the K-model, as described above.

3.1.2. Wave measurements available

Field data from the Sylt–Rømø Bight in 1996 and 1997 were compiled by GKSS within the PROMISE project. Wind, wave, and current measurements are available for April 1997 at the two measurement piles P1 Lister Ley and P3 Rømø Dyb. One-dimensional wave-energy spectra were obtained from floater time series at 10-min intervals. From the spectra, wave height and different wave-period parameters were computed by integration. The quality of wave-height measurements at P3 Rømø Dyb could be cross-checked by comparing with a nearby Waverider buoy. The Waverider data are available in 1-h intervals. Throughout the month of April 1997, the two independent wave-height measurements at P3 agreed very well. This supported the credibility of wave height measurements. The floater wave heights and T_{m1} periods at both stations

roughly fulfil the energy-frequency relations following from a TMA spectral shape. This gave a first quality check for the period measurements. The periods obtained from the Waverider data agreed well with the floater data from P3 except for situations with wave heights below 0.2 m. Here, the Waverider periods were generally larger than the floater periods.

3.1.3. Model results

The primary objective of the April 1997 hindcast experiment was the comparison with field data. For this reason, the presentation of results will be confined to selected time series of waves and currents and validation statistics at the two field stations.

3.1.3.1. Selected time series. Time series of waves and currents are given in Figs. 3 and 4 for the period 10th to 16th April 1997. The maximum wind speed in April occurred in this period (cf. Fig. 2). Wind directions were west to north, and the peak wind velocity was from the northwest. Wave measurements at P1 were interrupted for a few hours after 00:00 13th April.

After correcting for small time-independent offsets (cf. Section 2.3), measured and modelled water levels agreed very well at P1 and P3. For this reason, we decided not to show water-level time series, but indicate that current model results have been very satisfactory with respect to water levels. Further details are given in Appendix A. The approximate water level at low tides was 2 m at both sites. The variation in tidal levels was roughly 2.3 m.

The quality of currents input into the wave model at P1 can be assessed from the third and fourth panels of Fig. 3. The TRIM model was successfully validated in Sylt–Rømø Bight applications, see Appendix A. Here, the quality of input current fields for the wave model can be seen. Note that these currents are post-processed results from the current model, which have been reduced in spatial resolution from 100-m to the 500-m resolution of the wave-model grid. The modelled current velocities agree well with measurements in the ebb part of the tidal cycle. The structure of the measured flood part of the tidal-cycle — a short peak followed by a sharp decline in current velocity — is not reproduced well in the model input current field. Model current directions are reproduced reasonably well in the wave model input. The quality of current input to the wave model at P3 is comparable to P1, see panels three and four of Fig. 4.

Model results for significant wave height at P1 agree well with floater measurements at peak wind speeds, but are too high for moderate wind speeds in between peaks. For low wind speeds, agreement of model and measurements is better. Differences of significant wave heights from model runs with current input and without are small at P1. The model with currents is systematically higher for the flood part of the tide. At the ebb part of the tide, no difference can be seen. This qualitative result was also obtained in the NW20 case study at location P1, it will be discussed in Section 4.3. Differences in significant wave height within the displayed period are at most 7 cm, or 9%.

Model results for T_{m1} periods at P1 agree well with measurements. The influence of currents on the wave model results is more obvious for the T_{m1} periods. The tidal modulation is reproduced remarkably well by the wave model with current input for the measured periods at P1. Agreement with measurements improves significantly by

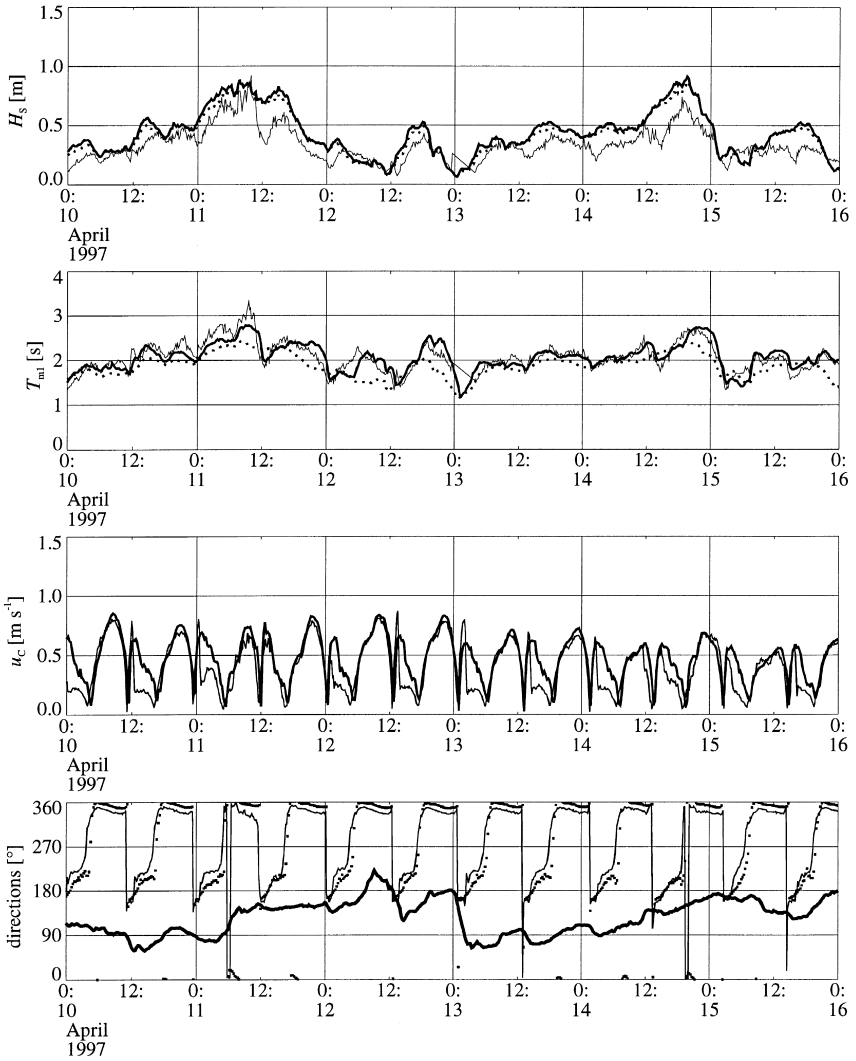


Fig. 3. Time series of wave and current parameters for a selected period of the April 1997 hindcast at location P1 Lister Ley. The top two panels display significant wave height and T_{m1} period. Thick lines are model results with current input, dotted lines model results without. Thin lines are float measurements. The third panel displays model input current velocity as thick line, measured current velocity as thin line. In the bottom panel, model input current directions appear as dotted, measured current directions as thin line. Modelled mean wave directions are displayed as thick line.

including currents in the wave model. Taking currents into account, the T_{m1} periods can change by as much as 0.5 s at location P1. Model mean wave directions have been added to panel four to show that current effects on T_{m1} periods are largest for current directions parallel to and opposing the wave directions.

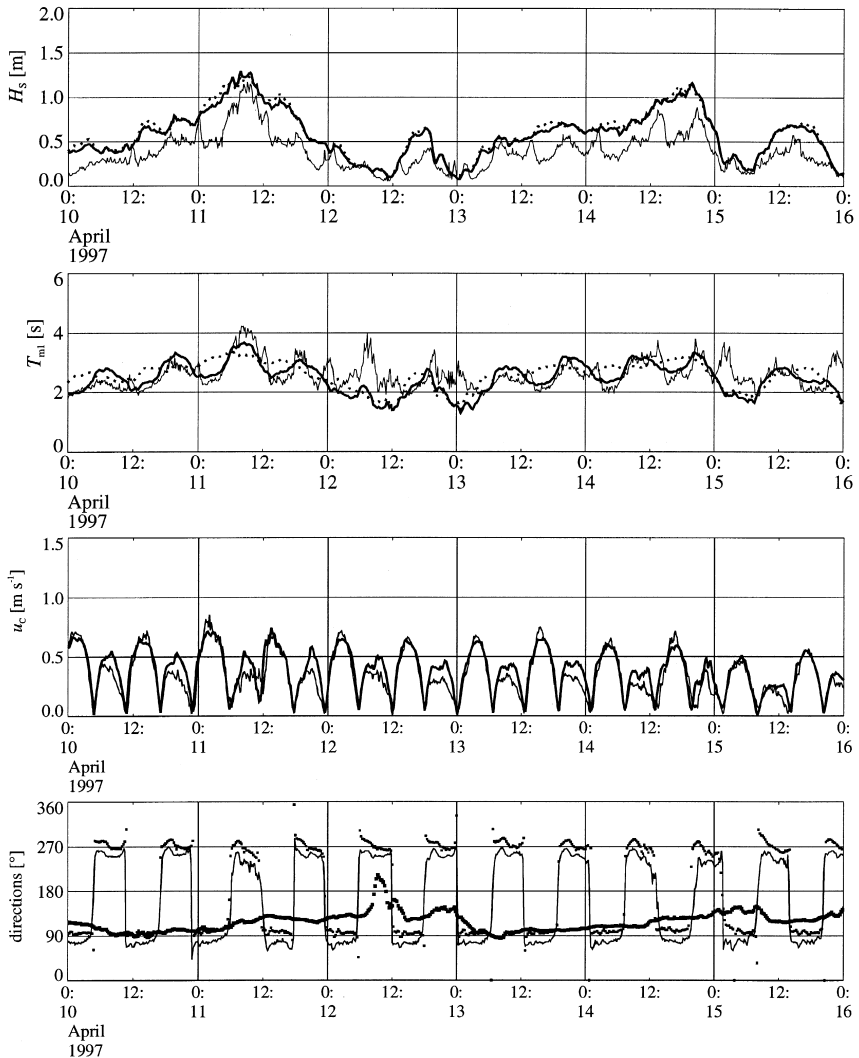


Fig. 4. Time series of wave and current parameters for a selected period of the April 1997 hindcast at location P3 Rømø Dyb. The top two panels display significant wave height and T_{m1} period. Thick lines are model results with current input, dotted lines model results without. Thin lines are floater measurements. The third panel displays model input current velocity as thick line, measured current velocity as thin line. In the bottom panel, model input current directions appear as dotted, measured current directions as thin line. Modelled mean wave directions are displayed as thick dotted line.

Fig. 4 displays wave and current parameters at pile P3. The overall picture of wave-model results for wave heights is similar to P1. At measured peaks, the wave heights are reproduced well but generally a positive bias can be expected. The influence of currents on modelled wave heights is similarly small as seen at location P1. At P3,

the opposite effect occurs: during the flood wave heights computed with current input are systematically lower than computed without. During the ebb, no differences can be seen in the results. As for P1, this behaviour at location P3 was also observed in the NW20 case study. Differences in modelled wave heights from the two model versions are at most 10 cm, or 10%.

The magnitudes of measured T_{m1} periods at P3 are reproduced well by both model versions except for when there is little wind and wave heights are below 20 cm. Here, measured T_{m1} periods are larger, e.g. an increase to 4 s during 03:00–12:00 12th April. The models do not reproduce this increase in period. It is likely that the observed increase in period is not artificial, since it also appears in the Waverider measurements close to P3 (not shown here). It can be attributed to the influence of incoming residual wave energy from the open sea, which becomes noticeable in places where the wind-sea is low. This explanation is supported by the fact that the effect was not observed at P1, which is less exposed to the open sea. The residual wave energy is reproduced inadequately by the wave model, and this will be discussed in the next subsection. At moderate and higher wind speeds, the wave-model version with current inclusion reproduces the tidal modulation of measured periods well, as was the case for location P1. Differences in both model versions can be well above 0.5 s, or 25%, at P3.

3.1.3.2. Validation statistics. Validation of wave-model results against measurements from floaters at locations P1 and P3 and Waverider at location P3 are given in Tables 1 and 2. The tables display statistics for significant wave height and T_{m1} period, computed with and without current input. This allows a quantitative and objective assessment of the influence of currents on wind waves as seen at the two locations. Wave-modelling results from the entire hindcast period ranging from 12:00 2nd April to 00:00 28th April 1997 have been used to produce the statistics. The hindcast period was fixed by the availability of measurements. The fairly dense field data set ensures statistical significance since it considers roughly 2000 data points in the comparison with floater measurements and roughly 750 data points for Waverider measurements. The definitions of statistical parameters are given in Appendix B.

Table 1 contains the wave height statistics. Statistical parameters of results from the two model versions are similar. This was expected, as the current influence in the time series was weak. Biases are positive at all locations, but reasonably small: 5–7 cm at P1 and 12 cm at P3 for both measuring devices. Root mean square errors (RMSE) range from 10 cm to less than 20 cm. The scatter indices look fairly high with values from 30 to 40, resulting from low mean values of the measurements. The skill is always positive, ranging from roughly 0.2 to 0.6 for different stations and model versions.

Table 2 shows statistics for the T_{m1} periods. Since current effects were more obvious in the time series of this parameter, one can expect to see differences in the statistics for the two model versions. For location P1, the clear improvement in hindcast quality by considering wave-current interaction is reflected by a decrease in the magnitude of the bias, decrease in RMSE, and doubling of skill to 0.66. The internal variability of the floater time series includes tidal modulation and is expressed by the standard deviation of measurements. It is reproduced by the wave model with current input, but is too low for the model version without current input.

Table 1

Validation statistics for significant wave height for three stations within the Sylt–Rømø tidal basin. Statistics for the K-model with and without taking currents into account. See Appendix B for definition of statistical parameters

Location and field method	Number of points	Mean of data (m)	S.D. of data (m)	Currents in model?	S.D. of model (m)	Bias (m)	RMSE (m)	Scatter index	Skill
P1 floater	2061	0.31	0.15	yes	0.19	0.07	0.11	28	0.44
				no	0.18	0.05	0.10	27	0.58
P3 floater	2065	0.32	0.20	yes	0.27	0.11	0.17	39	0.31
				no	0.27	0.12	0.18	44	0.19
P3 Waverider	757	0.38	0.25	yes	0.28	0.12	0.17	30	0.56
				no	0.29	0.12	0.18	33	0.50

Table 2
Validation statistics for T_{m1} period, annotation as for Table 1

Location and field method	Number of points	Mean of data (m)	S.D. of data (m)	Currents in model?	S.D. of model (m)	Bias (m)	RMSE (m)	Scatter index	Skill
P1 floater	2061	1.99	0.34	yes	0.35	−0.04	0.20	10	0.66
				no	0.30	−0.19	0.28	11	0.32
P3 floater	2065	2.47	0.51	yes	0.56	−0.26	0.65	24	−0.59
				no	0.54	−0.24	0.65	24	−0.59
P3 Waverider	757	2.81	0.52	yes	0.58	−0.48	0.86	25	−1.78
				no	0.55	−0.46	0.86	26	−1.78
P1 floater ($H_S > 0.2$ m)	1354	2.53	0.46	yes	0.45	−0.06	0.38	15	0.32
				no	0.44	−0.06	0.46	18	0.00
P3 Waverider ($H_S > 0.2$ m)	478	2.82	0.42	yes	0.40	−0.18	0.37	11	0.25
				no	0.34	−0.15	0.44	15	−0.09

The validation statistics for T_{m1} periods against floater and Waverider measurements at P3 reflect the poor performance of the hindcast where low wind-waves are present with residual low-frequency wave energy. The RMSEs are large, exceeding the standard deviations of the measurements and thus leading to negative hindcast skills. To show that better performance occurs when wind-waves are present, the table gives additional statistics for when corresponding wave heights are above 20 cm. The hindcast skill of the model with currents is now positive and, as at P1, substantially better than for the model without currents.

3.1.4. Modulation of measured wave heights with semi-tidal period

In Fig. 4, it is observed that throughout the measured wave height time series, a periodic modulation with semi-tidal period exists. The measured wave heights exhibit local maxima shortly after high tide and low tide, i.e. after current-velocity minima independent of current direction. This is obvious during 13th to 15th April. This modulation of wave heights is not reproduced by either version of the wave model.

3.2. Case studies

3.2.1. Wave parameter fields

Figs. 5 and 6 characterise the wave climate in the Sylt–Rømø Bight, showing fields of significant wave height and T_{m1} period for the E20 and NW20 cases at selected high tides. Some general features are listed below.

(1) Waves in the inner parts of the bight are strongly depth-dependent, and are reflected in the spatial patterns of the wave parameters.

(2) For the E20 case, results consistent with fetch-limited growth and slanted fetch conditions are visible outside the bight. These are disturbed by increased fetch at the bight entrance. Fetch-limited growth within the bight is strongly depth-dependent.

(3) In the NW20 case, wave heights and periods at the western and northern boundaries to the open North Sea are fixed by specified time-constant boundary spectra. Outside the bight, wave heights decrease with increasing distance from the boundaries whereas the periods increase. This is caused by a dynamic balance of shallow-water dissipation and shoaling. The shoaling increases T_{m1} , whereas total energy is decreased by enhanced dissipation in shallower water. This explanation is supported by the fact that rising T_{m1} periods coincide with steep depth gradients present at beach on the west side of Sylt and at the flats in front of the bight entrance.

(4) In the NW20 case, refraction of propagating waves into the bight entrance is visible as variations in the mean wave directions. Since a high-tide situation with marginal tidal currents is displayed in the figure, it can be inferred that the refraction is caused by depth gradients.

3.2.2. Parameter difference fields

In order to indicate orders of magnitude of current effects on wave parameters and to show current-induced spatial patterns, differences of model results computed with current input and without are given in Figs. 7–9. Times were selected to show extreme

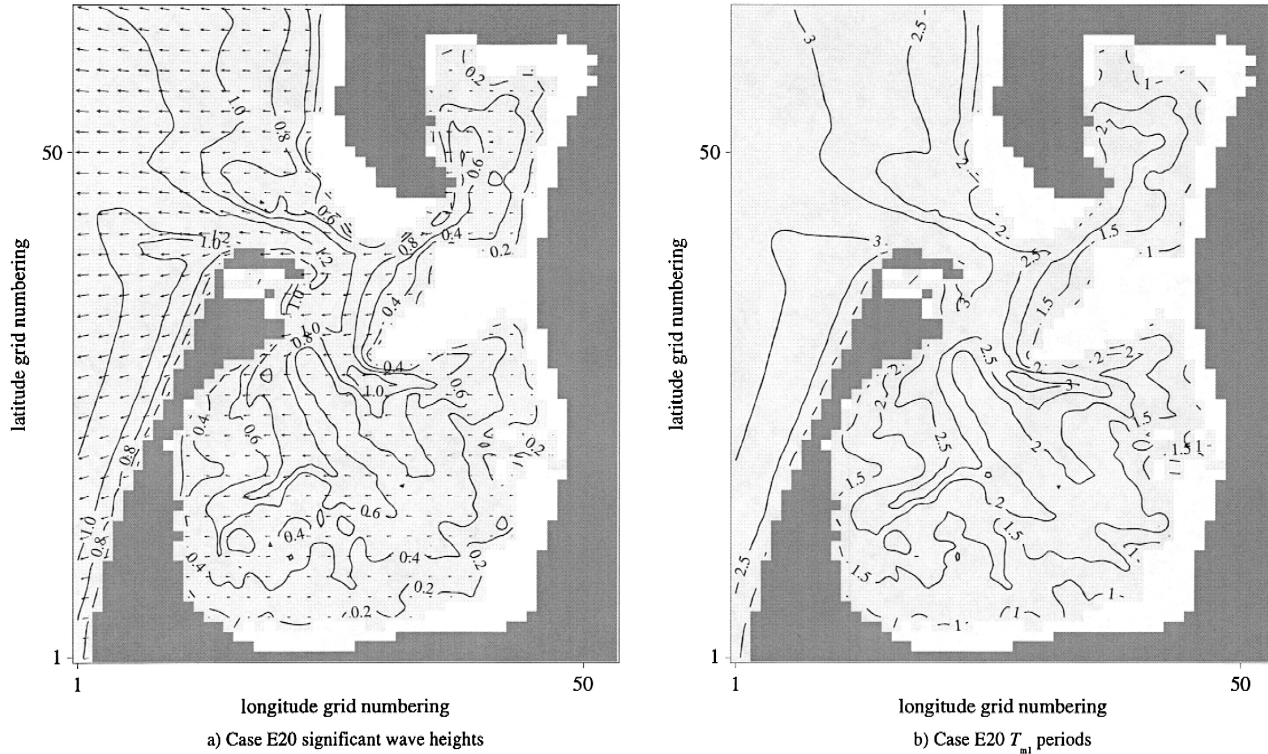


Fig. 5. Fields of wave parameters for the E20 case at a selected high tide. In panel (a), contour lines represent wave heights in metres. Arrows give wave directions. Arrow lengths are scaled proportional to significant wave height. In panel (b), contour lines give T_{m1} periods in seconds. Grey shading as in Fig. 1.

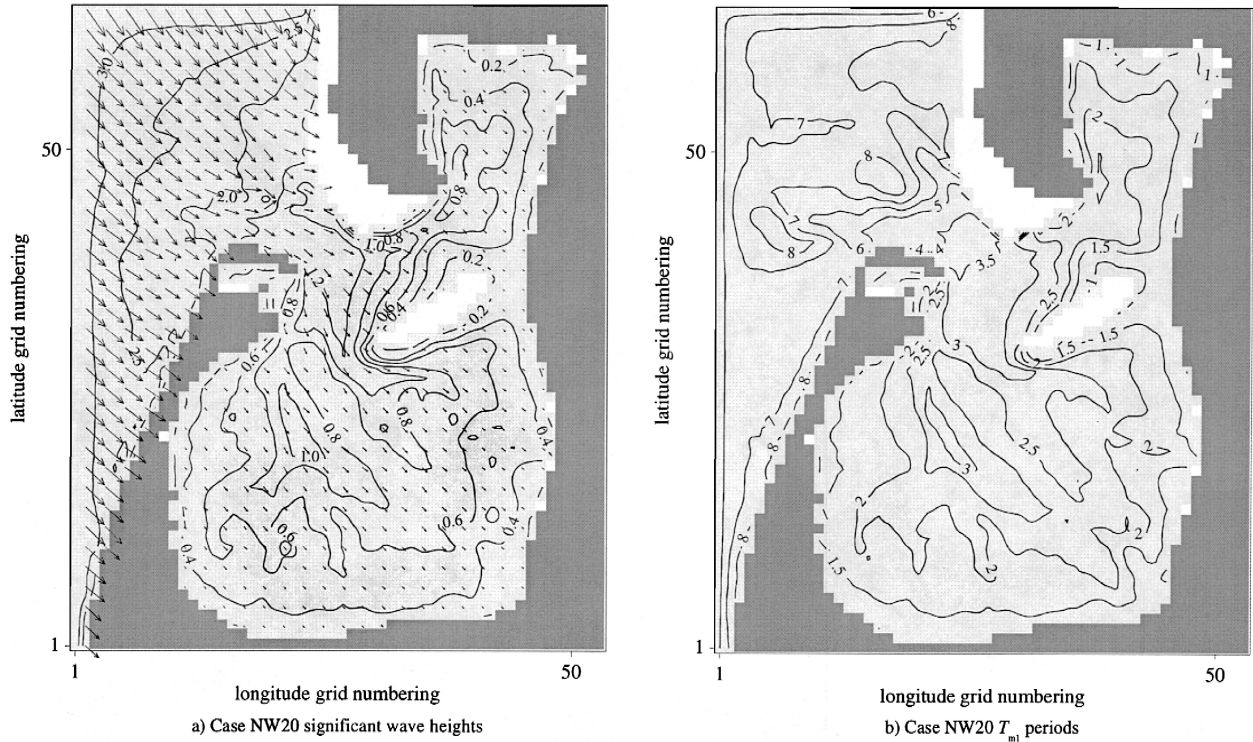


Fig. 6. Fields of wave parameters for the NW20 case at a selected high tide. In panel (a), contour lines represent wave heights in metres. Arrows give wave directions. Arrow lengths are scaled proportional to significant wave height. In panel (b), contour lines give T_{m1} periods in seconds. Grey shading as in Fig. 1.

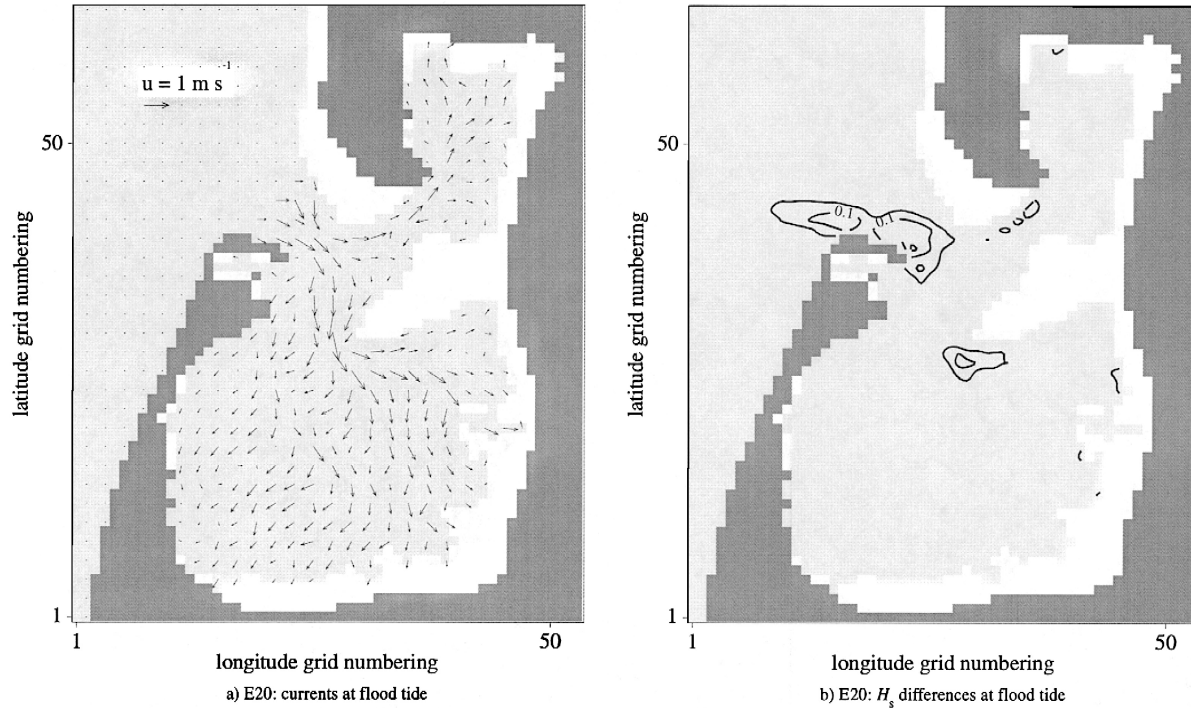


Fig. 7. Currents and difference field of significant wave height at a selected date — 1 h before high tide — for the E20 case. Contour interval is 0.05 m. Arrow lengths are proportional to current velocities.

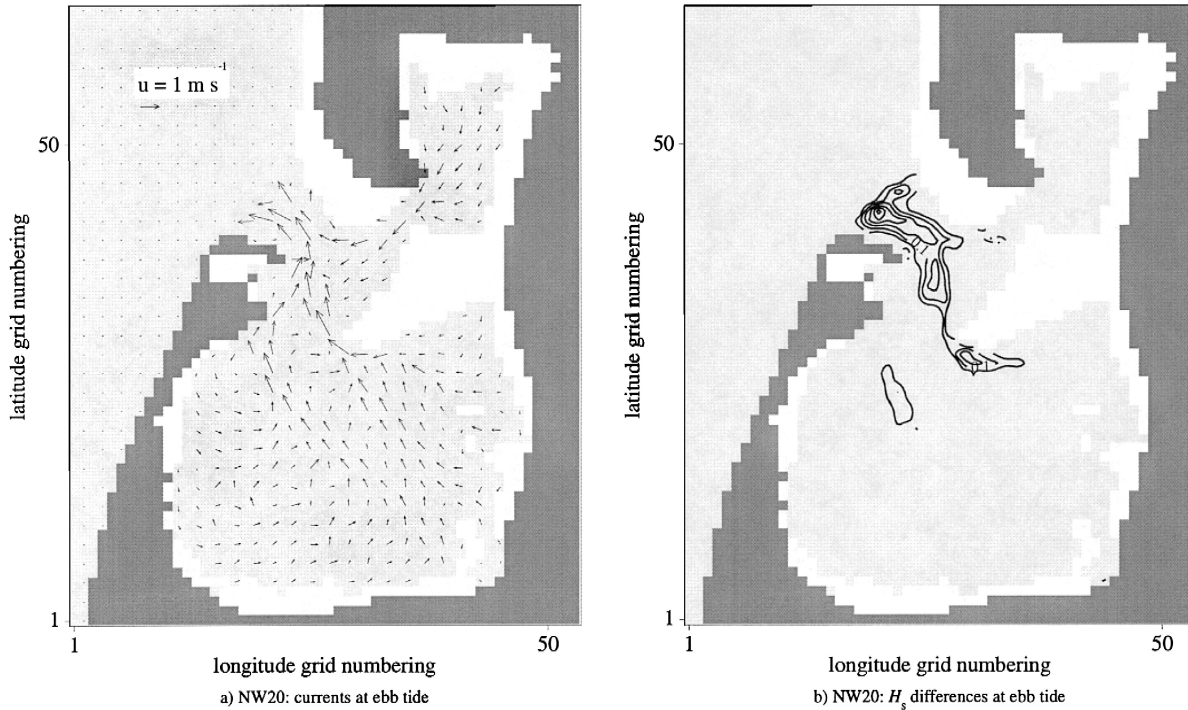


Fig. 8. Currents and difference field of significant wave height at a selected date — 2.5 h before high tide — for the NW20 case. Contour interval is 0.05 m. Arrow lengths are proportional to current velocities.

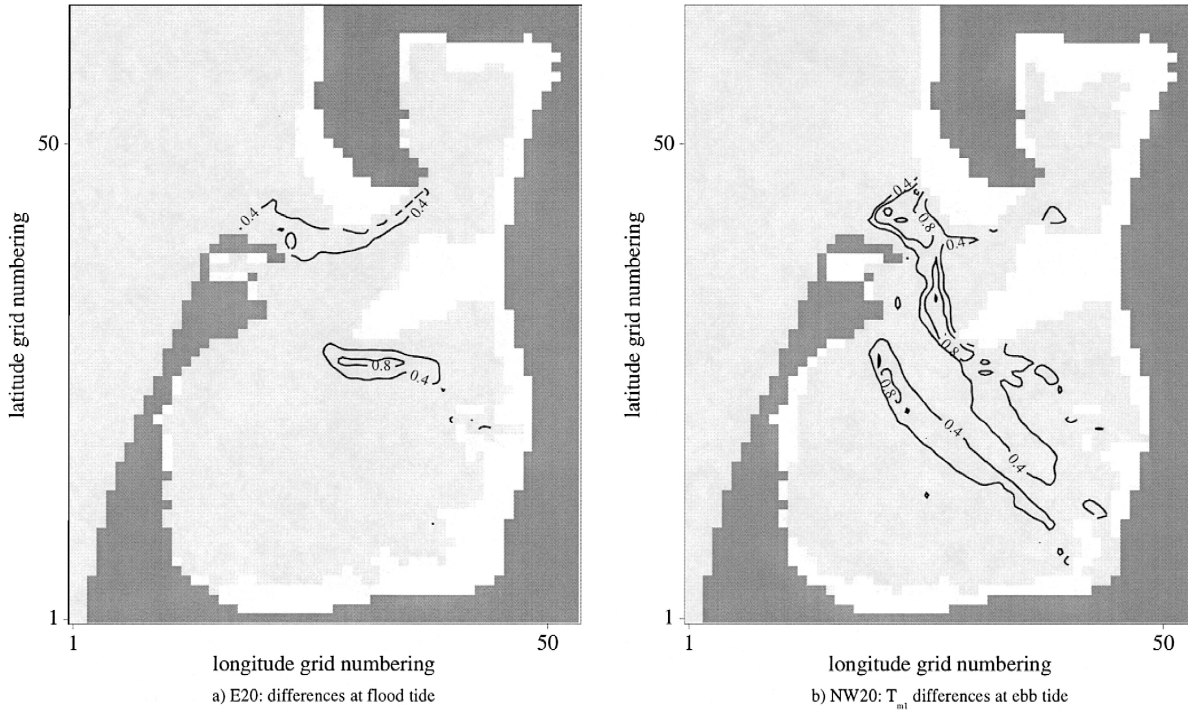


Fig. 9. Difference fields of T_{ml} periods. Dates correspond to Fig. 7 (panel a) and 8 (panel b). Contour interval is 0.4 s.

current influences on wave parameters. Features visible in the difference fields are indicated by the following. Magnitudes of current-induced variations are expressed as a percentage of the local parameter difference relative to the parameter value computed without currents.

(1) For the E20 case, panel (b) of Fig. 7 shows that wave heights can increase through current influence by 10 to 15 cm. Effects are visible only at the bight entrance and at Højer Dyb. For both, opposing currents are present in the fetch development of waves to the locations. At the bight entrance the relative magnitude of the current-induced variation is 13%, at Højer Dyb it is 12%.

(2) Current impacts on wave parameters are generally larger in the NW20 case. Wave height increases by 30 cm, or 20%, at the bight entrance panel (b) of Fig. 8, but significant increases are also visible within the bight up to Højer Dyb. Here, the relative change is 17%.

(3) The T_{m1} periods are influenced more significantly by currents (Fig. 9). Comparing these with the corresponding current fields, the changes depend on the local current components parallel to as well as opposing the mean wave direction.

(4) For T_{m1} periods in the NW20 case, current-induced increases are well above 1 s at the bight entrance and north of Højer Dyb. The relative increase is 27%.

The selected parameter difference fields suggest that the increases in wave height and T_{m1} period are due to the impact of currents. Conversely, decreases in these parameters can occur. See, for example, the discussion of time series in the next section. Corresponding figures have been omitted for brevity.

3.2.3. Selected time series

To indicate various tidal effects on wave parameters, time series of wave and current parameters at P1 Lister Ley are presented. The length of the time series covers two tidal cycles. Characteristic features related to tidal impacts, in particular current impacts, on wave parameters visible in the time series are described below.

(1) Fig. 10 displays parameters at location P1 Lister Ley for the E20 case. A distinct tidal modulation of significant wave height and T_{m1} period is visible, but the current influence is rather small, as can be seen by similar curves for both model versions (with current input and without). The mean wave direction changes through current influence by 16° at most. The tidal modulation of this parameter without currents is very small. For both flood and ebb tide, the mean wave direction is perpendicular to the current directions.

(2) Fig. 11 gives time series for the NW20 case at location P1 Lister Ley. During the flood semi-cycle, current directions change continuously from southeast to west. Current velocities during flood also exhibit a similar temporal evolution. Wave parameters are modulated by tides, as seen in the E20 case. However, a distinct ebb-flood asymmetric current variation of wave heights is also present in this instance. According to the model version with currents, wave heights are larger during flood; during ebb no difference is visible. An effect of the resembling was observed at P1 in the hindcast experiment, cf. Section 3.1. An explanation will be attempted in the discussion, Section 4.3. The T_{m1} periods are enhanced in the presence of opposing currents less strongly decreased by parallel currents.

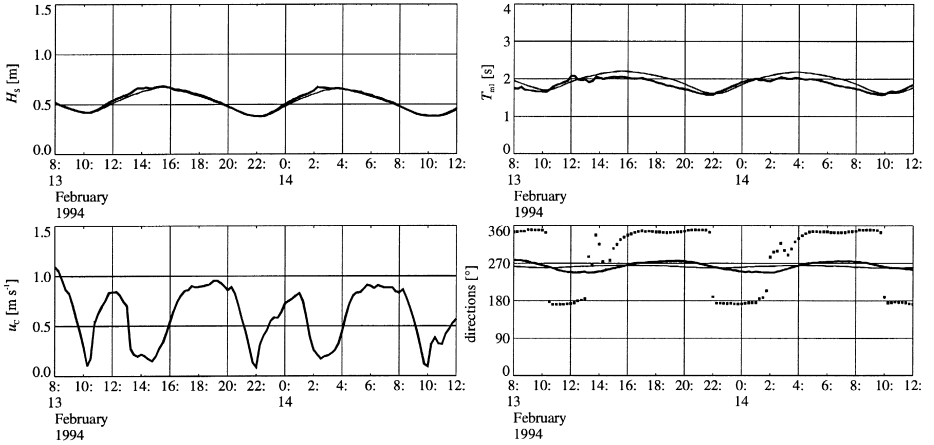


Fig. 10. Time series of wave and current parameters for the E20 case at location P1. Wave parameters computed with current input are given as thick lines, without currents as thin lines. The current direction is given as a dotted line (bottom right panel).

In the presented time series it has been obvious that current impacts appear in a systematic manner in the course of the tidal cycles: effects visible in the two cycles presented are roughly the same.

3.2.4. Selected spectra

In order to visualise principal current impacts on wave spectra, a selection of two-dimensional wave spectra for the NW20 case at two locations is given in Fig. 12.

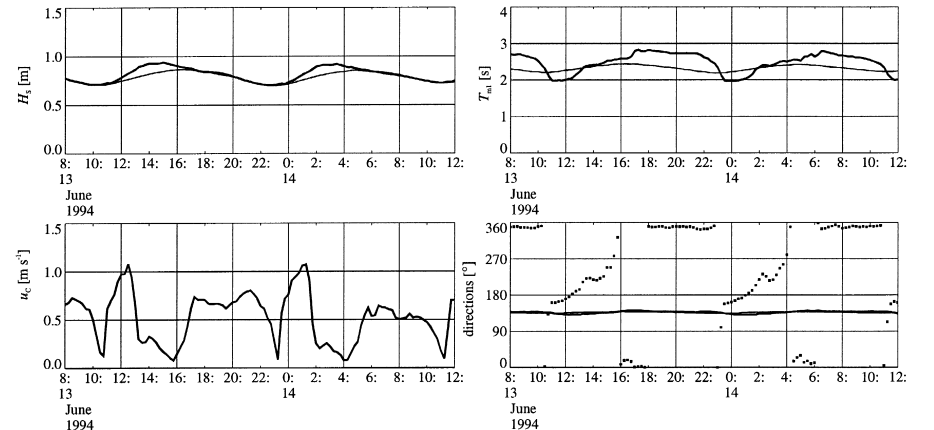


Fig. 11. Time series of wave and current parameters for the NW20 case at location P1. Line styles are as in Fig. 10.

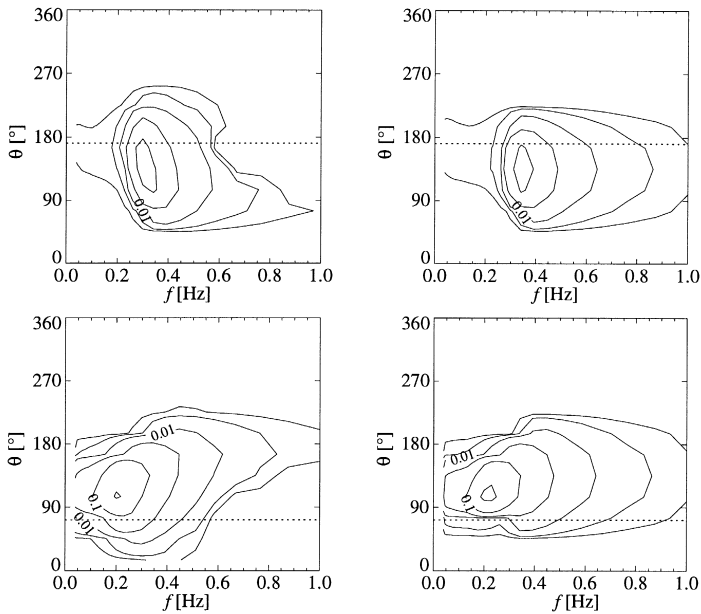


Fig. 12. Two-dimensional wave spectra of case NW20 at a selected date (2.5 h before low tide), at Lister Ley (upper panels) and Rømø Dyb (lower panels). Left panels give spectra computed with currents, right panels without currents. Contour line stepping is in logarithmic scale. Labels give spectral energy densities in $\text{m}^2 \text{Hz}^{-1}$. Dotted lines indicate wave directions opposed to local current directions.

Left panels display results obtained with current input, right panels without. As for the time series, this enables direct visualisation of current impacts. The contour intervals in the plots are logarithmic.

At the time chosen, strong ebb currents were present. At both stations, current directions opposed the wave directions in specific spectral bins. The spectra therefore exhibit ‘indentations’ in the directions where opposing currents induced Doppler shifts to the energy in the spectral bins. Spectral peaks are slightly shifted to lower frequencies. Spectra computed with currents are broader at all locations.

The influence of low-frequency wave energy from the open North Sea can be seen in the spectra, but it is small. Its distinctiveness in the plots is a result of the logarithmic contour intervals.

4. Discussion

4.1. Validation of the K-model

The validation statistics of model results against field data allow the quality of the model to be assessed. Statistical validation is a standard method in ocean wave modelling (see for example SWIM, 1985). For small-scale coastal applications, how-

ever, validation studies based on statistical analysis of wave parameters with time evolution are sparse in the literature. For this reason, values for statistical parameters from this study cannot be compared with performance of other models. Ris (1997) reported statistics of SWAN results against measurements in two coastal applications. However, the statistics have a different meaning since the stationary SWAN version was used in this study; samples are comparisons of modelled and measured data obtained from various field stations at the same point in time. Wolf and Rosenthal (1999) present validation statistics of an application of the hybrid-parametric wave model HYPAS (Günther and Rosenthal, 1983) to a small-scale coastal system adjacent to the Baltic Sea (the Odra lagoon). In this system tidal influences are negligible. This justifies the use of HYPAS in which current effects cannot be considered. We conclude that a statistical validation of a non-stationary wave model in a small-scale tidal system as presented in this study has not been reported before. The K-model's biases and RMSEs are small in comparison to ocean-wave-model statistics, but this is obvious since the magnitudes of the parameters themselves are also much smaller. Scatter indices are large in comparison to ocean-wave-model statistics, but this results from very low mean values of measurements obtained during the hindcast period. Values obtained for the hindcast skills are positive except for wave periods at station P3. Therefore the K-model's performance is considered as satisfactory. This is a step forward, since long hindcasts of waves in small-scale tidal environments have not been reported before. In this study, tidal-current-induced modulations of wave-period parameters have been reproduced for the first time in a quantitative manner. This has led to a distinct improvement in hindcast skill.

The negative skill values for T_{m1} statistics at station P3 are unsatisfactory. The exclusion of data points connected with low wave heights is questionable in a thorough statistical validation, but shows that the hindcast performance for wave periods is significantly reduced only in situations where wind-waves are negligible and residual low-frequency energy from the open sea pushes up the period parameters. A wave model has principal shortcomings in this case, since division by small numbers (when the total energy is low) is involved in the calculation of T_{m1} periods. This is not an explanation for its deficiency, since this would lead to large scatter instead of underestimating T_{m1} . One explanation is the limited spatial and directional resolution in the model set-up, cf. Section 2.3. Due to this limitation, an excessive part of incoming wave energy is dissipated at the narrow entrance of the bight.

4.2. Measured semi-tidal modulation of wave heights

The semi-tidal modulation of wave heights apparent at location P3 Rømø Dyb can be attributed to an influence of current modulus on wave height. It was not observed at station P1. The effect was not resolved in the K-model output. One explanation is an unrecognised influence of current modulus in the source functions. For instance, the wind input can be altered by a decrease in surface roughness in the presence of currents, thus leading to a decrease in momentum flux. Bottom friction dissipation is influenced by the current modulus according to theories described in Hasselmann and Collins (1968) and Hasselmann et al. (1973). Finally, wave turbulence interaction can be

enhanced by higher turbulence levels in the presence of currents. This effect can easily be parameterised in the K-model by a current modulus dependence of the eddy viscosity entering the dissipation constant, cf. Section 2.1. The analysis is outside the scope of the present study, but it is recommended for future work.

4.3. Case studies: influence of currents on wind waves

The results presented for the two case studies have revealed tidal impacts on wave parameters in the Sylt–Rømø Bight. This is expected from the discussion of principal effects of inhomogeneous and non-stationary external fields in Section 2.1. Water depth induced tidal modulations visible in the time series resulted from depth-dependent source functions and varying fetches due to dry-falling areas. Current-induced Doppler shifts had a major impact on period parameters and spectral shape. A less distinct influence of non-local current effects led to considerable changes of wave heights and directions. In the following paragraphs, some detailed examples will be discussed.

Local current-induced frequency shifts, i.e. Doppler shifts within the frequency-direction spectra, are mainly responsible for variations in the T_{m1} periods. This can be deduced from the systematic dependence of shifts on current directions, visible in the parameter difference fields as well as in the time series. The fact that T_{m1} variations are larger in magnitude for opposing currents, see Fig. 4, is explained by the non-linearity of the dispersion function (Eq. (13)).

The Doppler shift also has a large impact on the current-induced variation of spectral shape. This mechanism explains the observed energy shifts to lower frequencies in spectral direction bins opposed to current directions. This is responsible for the observed broadening (Fig. 12). Shifted energy in directional bins opposed to the current accumulates at lower frequencies, thus raising the ‘flanks’ of the spectrum in the vicinity of the peak.

Current-induced variations of wave heights are in most cases less distinct than for T_{m1} periods, because the discussed Doppler shifts are energy-conserving and thus do not affect significant wave height. Advection of wave energy with currents coming from the bight entrance is probably the cause for increases in wave height during flood in the NW20 case at P1 (cf. Fig. 11, and in the hindcast, Fig. 3). An increase of effective fetch for opposing currents enlarges wave heights at the bight entrance and Højer Dyb for case E20, as seen in the difference field, Fig. 7. Variations in wave height at the bight entrance shown in Fig. 8 are mainly caused by current shoaling of incoming waves from the open North Sea. This mechanism increases wave heights in rising gradients of opposing currents, and decreases wave heights in rising gradients of currents travelling along the waves.

Of all wave parameters shown in the time series, mean wave directions are least influenced by tidal currents. The only considerable impact is seen in the time series of case E20 at P1, Fig. 10. Mechanisms which can contribute to the variation of mean wave direction are: advection of wave energy by currents, current refraction, and an interplay of wind input and current-advection propagation leading to effective angled-fetch conditions. A current impact depending on local properties, such as Doppler shifts, is only possible through wave blocking leading to an inversion of propagation direction for

energy in certain spectral bins. Current-induced changes in wave parameters were larger for the NW20 case than for the E20 case. Different behaviour for the two case studies was expected since relative angles of current directions and mean wave directions were different for the two cases. The significance of current impacts in relation to water-depth impacts varies with location, meteorological situation, and regarded wave parameter. Currents may impact on tidal modulations at any location. Regardless of the circumstances, neither tidal currents nor tidal depth variations can be classified as the dominant mechanism for tidal modulation of the sea state.

The modelled current effects on wind-waves in the Sylt–Rømø Bight can be compared with results from a similar study in a Dutch coastal environment (Friesche Zeegat) (Ris, 1997). To detect current effects Ris compared wave-model results obtained with and without current input. The simulations were carried out with SWAN in stationary mode. The stationary treatment was justified in the Friesche Zeegat application, since in that study emphasis was placed on the analysis of approaching waves from the open sea into the tidal inlets. The magnitude of current impacts on wave parameters reported by Ris is similar to the results described in this paper: a major impact on T_{m1} periods was reported, whereas significant wave heights were influenced less distinctly. Variation of mean wave direction was the same order of magnitude as reported here. Results of the two studies are generally consistent. Tidal influence on significant wave height in the Sylt–Rømø Bight was also investigated with a coastal wave model by Winkel (1994), but only impacts of varying water depths were analysed.

5. Concluding remarks

Results from a 1-month hindcast of wind waves in the Sylt–Rømø Bight led to the following conclusions.

1. The K-model was successfully validated at two locations within the Sylt–Rømø Bight. A comparable performance can be expected in applications to similar coastal systems and in forecast mode, since the K-model was not recalibrated to match the field data.
2. A substantial improvement of wave period hindcast in the Sylt–Rømø Bight by inclusion of tide-current effects was demonstrated. This was proved in a quantitative and objective manner by validation against field data.
3. Current effects on significant wave height at the two field stations were insignificant for most of the time. Therefore, an improvement of hindcast quality for this parameter could not be proved by validation statistics against measurements.

The following conclusions can be drawn from the E20 and NW20 wave-modelling case studies in the Sylt–Rømø Bight.

1. The K-model can be used successfully for coupled investigations of coastal tidal environments.

2. The case studies revealed considerable and systematic tide impacts, in particular tide-current impacts, on integrated wave parameters and spectral shape of wind waves in the Sylt–Rømø Bight.

As a result of this work, we recommend that a sensitivity study be performed on the relevance of current influences on the sea state in a particular coastal wave modelling application. On the basis of these, it can be decided whether or not to consider currents within the complete investigation. The K-model can readily be used for such studies.

Acknowledgements

Field measurements presented in this paper were carried out by co-workers of the Institute of Hydrophysics, GKSS-Forschungszentrum Geesthacht, Germany. The authors are also indebted to Dr Arno Behrens and Gerhard Gayer for their work on the current modelling effort described in Appendix A. This work, as well as the wave modelling study was performed within the European Union MAST III project PROMISE, MAS3-CT9500025, 'PRE-Operational Modelling In the Seas of Europe'. Corresponding financial support is gratefully acknowledged.

Appendix A. Current modelling in the Sylt–Rømø Bight

The aims of modelling current and water level were to support various PROMISE measurement campaigns, to establish a complete reference data set and to provide input fields for the wave modelling investigations. This appendix briefly describes the model set-up, the preparation of boundary values using remote tide gauge data, and two different model applications.

A.1. Model set-up

The 2D version of the hydrodynamic model TRIM2D (Casulli, 1990, Casulli and Cheng, 1992, Casulli and Cattani, 1994, Cheng et al., 1993) was applied to the Sylt–Rømø Bight. The bathymetry of the Sylt–Rømø Bight, with a resolution of 100×100 m, was compiled from nautical and bathymetric charts of the Wadden Sea as well as from echo soundings. For the model runs, all water depths westwards from the model boundary between the islands of Sylt and Rømø were set to a 'dummy' value indicating that water here was outside of the computational domain (Fig. 1).

At this open boundary the model was forced by time series of water level variations every 15 min. These data series were prepared from routine measurements taken at gauges at Westerland and Lister Deep because direct measurements were not available at the model boundary. Lister Deep is about 7 nautical miles off the open model boundary. These tidal elevations were applied at the boundary with a delay of 45 min to allow for the propagation time. In those cases where data from Lister Deep were not

available, we used data from Westerland. These measurements were transferred to the Lister Deep location by a linear transformation, determined from simultaneous measurements at both sites. Forcing the model at the open boundary by measured data had the advantage that these boundary values reflected the atmospheric forcing for water levels and current fields in the German Bight.

Further details of the model set-up are described in Behrens et al. (1997).

A.2. Current and water level atlas

Time series of wind speed and direction measured at the Westerland meteorological station, operated by the German Weather Service, were inspected. Periods of approximately constant wind conditions over a couple of tidal cycles were selected for 24 reference cases (eight wind direction sectors of 45° and three wind speeds of 5, 10, and 20 m s^{-1}). Comparisons of model results with water level measurements, which were available from two locations inside the bight for each of the 24 periods, showed very good agreement. The current and water level fields of all of these reference cases are documented in Behrens et al. (1997) and are available on CD-ROM in the form of an atlas.

A.3. April 1997 hindcast

The second application was a hindcast of the PROMISE field campaign in April 1997. These results were compared to measurements at site P1 and P3. The fourth panel in Fig. 3 shows modelled and measured current directions during April 1997. Instead of a regular change in current direction — to the north during ebb and to the south during the flood — we observe changes in direction corresponding to the behaviour of an eddy. The direction gradually changes from approximately 180° during eddy generation, to 220° during dissipation, followed by a sudden veering to approximately 350° during the subsequent ebb. The third panel of Fig. 3 shows the corresponding current speed at pile P1 from the same period as depicted in the fourth panel of Fig. 3. While the curve of model results agree well with the measured values during the ebb semi-cycle, the differences are bigger during the flood-cycle. Both the measurements and simulation show fast increase in speed as soon as the flood-cycle begins. When the eddy starts to develop the measurements show a much sharper drop to lower current speeds than the model does. If we assume that the measured values are representative of the total water column, it seems that in nature the current speeds during flood adjust very quickly to the general circulation pattern with slower water flow from the shallower parts of this area.

Although it is difficult to compare single point measurements taken at a certain water depth with model results representing a water column over a $100 \times 100 \text{ m}$ square, the results are very pleasing.

A.4. Conclusion

The model is capable of simulating the circulation and water level variation in the Sylt–Rømø Bight very well. The method of applying measured water level variations as

hydrodynamic boundary conditions at the narrow entrance to the Sylt–Rømø Bight proved to be an excellent tool to produce realistic model simulations.

Appendix B. Validation statistics parameters

In this section, definitions of statistical parameters used in Tables 1 and 2 are given. The ‘bias’ is given as difference of mean of model results to mean of measurements

$$\text{bias} = \bar{y} - \bar{x}. \quad (15)$$

Standard deviation of modelled data y to measured data x is given by

$$\sigma = \sqrt{\frac{1}{n-1} \sum_{i=1}^n ((x_i - \bar{x}) - (y_i - \bar{y}))^2} \quad (16)$$

n denotes the number of data points.

The scatter index is defined — involving the standard deviation — as

$$\text{scatter} = \frac{\sigma}{\bar{x}}. \quad (17)$$

The skill is given by

$$\text{skill} = 1 - \frac{\sum_{i=1}^n (y_i - x_i)^2}{\sum_{i=1}^n (\bar{x} - x_i)^2}. \quad (18)$$

A value of one indicates perfect skill. A value below zero indicates that use of the measured mean as prediction instead of model results leads to better hindcast performance. Further parameters appearing in the table are standard and therefore not listed here.

References

- Behrens, A., Gayer, G., Günther, H., Rosenthal, W., 1997. Atlas der Strömungen und Wasserstände in der Sylt–Rømø Bucht. GKSS Report No. 97/E/21, in German.
- Booij, N., Ris, R.C., Holthuijsen, L.H., 1999. A third-generation wave model for coastal regions: 1. Model description and validation. *J. Geophys. Res.* 104 (C4), 7649–7666.
- Cardone, V.J., Resio, D.T., 1998. An assessment of wave modelling technology. Proceedings of the 5th International Workshop on Wave Hindcasting and Forecasting, Melbourne, Florida, 468–495.
- Casulli, V., 1990. Semi-implicit finite difference methods for the two-dimensional shallow water equations. *J. Comput. Phys.* 86, 56–74.

- Casulli, V., Cattani, E., 1994. Stability, accuracy and efficiency of a semi-implicit method for three-dimensional shallow water flow. *Comput. Math. Appl.* 27, 99–112.
- Casulli, V., Cheng, R.T., 1992. Semi-implicit finite difference methods for three-dimensional shallow water flow. *Int. J. Numer. Methods Fluids* 15, 629–648.
- Cavaleri, L., Rizzoli, P.M., 1981. Wind wave prediction in shallow water — theory and application. *J. Geophys. Res.* 86, 10961–10973.
- Cheng, R.T., Casulli, V., Gartner, J.W., 1993. Tidal, residual, intertidal mud at (TRIM) model and its application to San Francisco Bay, California. *Estuarine Coastal Shelf Sci.* 36, 235–280.
- Donelan, M.A., 1995. Air–water exchange processes. Proceedings of IUTAM Symposium on Physical Limnology, Broome, Australia.
- Günther, H., Rosenthal, W., 1983. A shallow water surface wave model based on the TEXEL-MARSEN-ARSLOE (TMA) wave spectrum. Proceedings of the 20th Congress IAHR, Moscow, Russia.
- Günther, H., Rosenthal, W., 1995. A wave model with a non-linear dissipation source function. Proceedings of the 4th International Workshop on Wave Hindcasting and Forecasting, Banff, Canada.
- Günther, H., Hasselmann, S., Janssen, P.A.E.M., 1992. The WAM Model cycle-4.0. User manual. Deutsches Klimarechenzentrum Hamburg, Technical Report No. 4.
- Hasselmann, K., 1962. On the non-linear energy transfer in a gravity wave spectrum: Part 1. General theory. *J. Fluid Mech.* 12, 481–500.
- Hasselmann, K., Collins, J.I., 1968. Spectral dissipation of finite-depth gravity waves due to turbulent bottom friction. *J. Mar. Res.* 26, 1–12.
- Hasselmann, K., Barnett, T.P., Bouws, E., Carlson, H., Cartwright, D.E., Enke, K., Ewing, J.A., Gienapp, H., Hasselmann, D.E., Krusemann, P., Meerburg, A., Müller, P., Olbers, D.J., Richter, K., Sell, W., Walden, H., 1973. Measurements of wind-wave growth and swell decay during the Joint North Sea Wave Project (JONSWAP). *Dtsch. Hydrogr. Z., Suppl.* A8 (12), 95 pp.
- Hasselmann, K., Ross, D.B., Müller, P., Sell, W., 1976. A parametrical wave prediction model. *J. Phys. Oceanogr.* 6, 201–228.
- Holthuijsen, L.H., Booij, N., Ris, R.C., 1993. A spectral model for the coastal zone. Proceeding of the 2nd International Symposium on Ocean Wave Measurement and Analysis, New Orleans, USA, 630–641.
- Komen, G.J., Cavaleri, L., Donelan, M., Hasselmann, K., Hasselmann, S., Janssen, P.A.E.M., 1994. Dynamics and Modelling of Ocean Waves. Cambridge Univ. Press.
- Lin, R.Q., Perrie, W., 1997. A new coastal wave model: Part III. Nonlinear wave–wave interaction. *J. Phys. Oceanogr.* 27, 1813–1826.
- Luo, W., Sclavo, M., 1997. Improvement of the third generation WAM model (cycle-4) for applications in the near shore regions. Proudman Oceanographic Laboratory Internal Document No. 116.
- Makin, V.K., 1998. Air–sea exchange of heat in the presence of wind waves and spray. *J. Geophys. Res.* 103, 1137–1152.
- Monbaliu, J., Padilla-Hernández, R., Hargreaves, J.C., Carretero Albiach, J.C., Luo, W., Sclavo, M., Günther, H., 2000. The spectral wave model WAM adapted for applications with high spatial resolution. This volume.
- Phillips, O.M., 1981. Wave interactions — the evolution of an idea. *J. Fluid Mech.* 106, 215–227.
- Pierson, W.J. Jr., Moskowitz, L., 1964. A proposed spectral form for fully developed wind seas based on the similarity theory of S.A. Kitaigorodskii. *J. Geophys. Res.* 69, 5181–5190.
- Ris, R.C., 1997. Spectral modelling of wind waves in coastal areas. PhD thesis, Delft University of Technology.
- Ris, R.C., Holthuijsen, L.H., Booij, N., 1999. A third-generation wave model for coastal regions: 2. Verification. *J. Geophys. Res.* 104 (C4), 7667–7681.
- Rosenthal, W., 1989. Derivation of Phillips α -parameter from turbulent diffusion as a damping mechanism. In: Komen, G.J., Oost, W.A. (Eds.), *Radar Scattering from Modulated Wind Waves*. Kluwer Academic Publishers, pp. 81–88.
- Ross, J., 1995. Modellierung der Schwebstoffdynamik in einer Wattenmeerbucht (Königshafen/Sylt). PhD thesis, University of Hamburg, GKSS external report 95/E/56, in German.
- Schneggenburger, C., 1998. Spectral wave modelling with nonlinear dissipation. PhD thesis, University of Hamburg, GKSS external report 98/E/42.

- Schneggenburger, C., Günther, H., Rosenthal, W., 1997. Shallow water wave modelling with non-linear dissipation. *Dtsch. Hydrogr. Z.* 49, 431–444.
- Soulsby, R., 1997. *Dynamics of Marine Sands, A Manual for Practical Applications*. Telford, London.
- SWIM group, Bouws, E., Ephraums, J.J., Ewing, J.A., Francis, P.E., Günther, H., Janssen, P.A.E.M., Komen, G.J., Rosenthal, W., de Voogt, W.J.P., 1985. A shallow water intercomparison of three numerical wave prediction models (SWIM). *Q. J. R. Meteorol. Soc.* 111, 1087–1112.
- Tolman, H.L., 1991. A third-generation model for wind waves on slowly varying, unsteady and inhomogeneous depths and currents. *J. Phys. Oceanogr.* 21, 782–797.
- Tolman, H.L., 1992. Effects of numerics on the physics in a third-generation wind-wave model. *J. Phys. Oceanogr.* 22, 1095–1111.
- Tolman, H.L., Chalikov, D.V., 1996. Source terms in a third-generation wind wave model. *J. Phys. Oceanogr.* 26, 2497–2518.
- WAMDI group, Hasselmann, S., Hasselmann, K., Bauer, E., Janssen, P.A.E.M., Komen, G.J., Bertotti, L., Lionello, P., Guillaume, A., Cardone, V.C., Greenwood, J.A., Reistad, M., Zambresky, L., Ewing, J.A., 1988. The WAM model — a third generation ocean wave prediction model. *J. Phys. Oceanogr.* 18, 1775–1810.
- Winkel, N., 1994. *Modellierung von Seegang in extremem Flachwasser*. PhD thesis, University of Hamburg, GKSS external report 94/E/66, in German.
- Wolf, T., Rosenthal, W., 1999. Mesoscale wind and wave field modelling in the area of the Odra lagoon, in preparation.
- Young, I.R., 1998. Observations of the spectra of hurricane generated waves. *Ocean Eng.* 25, 261–276.
- Young, I.R., van Vledder, G.P., 1993. A review of the central role of nonlinear interactions in wind–wave evolution. *Philos. Trans. R. Soc. London A342*, 505–524.